JOURNAL OF COMPUTATIONAL PHYSICS **116,** 97–102 (1995)

Open Boundary Conditions for a Numerical Shelf Sea Model

DONG-JIAN GUO AND QING-CUN ZENG

Laboratory of Numerical Modelling for Atmospheric Sciences and Geophysical Fluid Dynamics (LASG)
Institute of Atmospheric Physics, Chinese Academy of Sciences, Beijing 100080, People's Republic of China

Received June 2, 1993; revised April 25, 1994

The barotropic numerical shelf sea model of the Institute of Atmospheric Physics, Chinese Academy of Sciences, is outlined first. For computing economy, a splitting method is applied by dividing the governing equations into three stages which are integrated with different time-steps. Open boundary conditions suitable for the different stages are derived from the locally linearized versions of the split governing equations. For the adjustment stage, the governing equations are converted to an equivalent set of characteristic equations, which represent waves propagating into or out of the computational domain. The outgoing waves are described by characteristic equations, while the incoming waves are suppressed by a nonreflecting boundary condition. For the development stage, general analytical solutions are found. At outflow points the boundary values at the upper time-level are obtained from data at the present time-level within and on the boundary via the analytical solutions, while the boundary values at inflow points remain constant in time. For the forcing-dissipation stage no boundary conditions are necessary. Numerical verification of the proposed open boundary conditions is described; the results are satisfactory.

1. INTRODUCTION

Numerical shelf sea models are frequently used to investigate the effects of wind stress on the sea-surface elevation and the current regime over a shelf sea area. Zeng *et al.* [1, 2] have developed a barotropic numerical shelf sea model (henceforth referred to as an IAP model), based on the two-dimensional primitive equations. In contrast to the other models of this kind, the IAP model has two unique features: (a) variable substitution is introduced into the governing equations, which leads the energy equation to a compact form; (b) the difference scheme designed preserves the properties of mass and energy conservation of original coastal flows involving open-sea boundaries. This model has been used to simulate wind-driven currents and storm surges in the Bohai Sea and the South China Sea. The results show that the model has good computational stability and accuracy [3, 4].

For computing economy, a splitting method is adopted in the IAP model, with which the governing equations are divided into three stages: adjustment, development, and forcing-dissipation. Naturally, the application of the splitting method requires open boundary conditions (OBCs) to be also split correspondingly. But this situation has not been investigated in previous studies. In this paper, OBCs suitable for the different stages are proposed.

The proposed OBCs are validated by two test cases. One is an experiment with a fluid contained within an infinitely long channel and the OBCs are applied at two cross sections along it. The other is the steady response of an open sea to a stationary cyclone where an analytical solution is available for comparison.

2. SKETCH OF THE IAP MODEL

In a local coordinate system (x, y, t), the two-dimensional primitive equations may be written as

$$\frac{\partial \boldsymbol{\nu}}{\partial t} + (\boldsymbol{\nu}\cdot\nabla)\boldsymbol{\nu} + f(\mathbf{k}\times\boldsymbol{\nu}) = -\nabla\phi - \gamma\boldsymbol{\nu} + \mathbf{F} \tag{1}$$

$$\frac{\partial \phi}{\partial t} + \nabla\cdot(gh\boldsymbol{\nu}) = 0, \tag{2}$$

where $\boldsymbol{\nu} = (u, v)$ is the depth-mean current vector; $\phi = g\zeta$ is the geopotential departure of the free sea-surface, ζ the sea-surface elevation; H and h are the undisturbed and total $(H + \zeta)$ water depths, respectively; $\gamma = 2.5 \times 10^{-3}|\boldsymbol{\nu}|^2/h$ is the bottom-friction coefficient; $\mathbf{F} = \boldsymbol{\tau}/\rho h$, $\boldsymbol{\tau}$ is the wind stress, ρ the density of the seawater; the other symbols are conventional.

In order to design the difference scheme which preserves the integral properties of the corresponding differential equations, we introduce a set of new variables via the following variable transformation

$$\Phi \equiv \sqrt{gh} = \sqrt{\phi + gH}, \quad \mathbf{V} = \Phi\boldsymbol{\nu}.$$

Thus, Eqs. (1)–(2) can be transformed into

0021-9991/95 $6.00

$$\frac{\partial \mathbf{V}}{\partial t} + (\boldsymbol{\nu}\cdot\nabla)\mathbf{V} + \frac{1}{2}(\nabla\cdot\boldsymbol{\nu})\mathbf{V} + f(\mathbf{k}\times\mathbf{V}) = -\Phi\nabla\phi - \gamma\mathbf{V} + \Phi\mathbf{F} \tag{3}$$

$$\frac{\partial \phi}{\partial t} + \nabla\cdot(\Phi\mathbf{V}) = 0. \tag{4}$$

Let S denote the flow domain under consideration, C is the edge of S, and $\mathbf{n}$ is the unit outward normal to C. The model Eqs. (3)–(4) have two important integral properties:

(a) Property of mass conservation,

$$\frac{\partial}{\partial t}\int\int_s \phi ds = -\oint_c (\mathbf{V}\cdot\boldsymbol{n})\Phi\, dc. \tag{5}$$

(b) Property of total energy conservation,

$$\frac{\partial}{\partial t}\int\int_s \frac{1}{2}(|\mathbf{V}|^2 + \phi^2)\, ds = -\oint_c \left[\frac{1}{2}(\boldsymbol{\nu}\cdot\mathbf{n})|\mathbf{V}|^2 + (\mathbf{V}\cdot\mathbf{n})\Phi\phi\right] dc + \int\int_s [-\gamma|\mathbf{V}|^2 + \Phi\mathbf{V}\cdot\mathbf{F}]\, ds. \tag{6}$$

Note that the energy expression on the left-hand side of Eq. (6) is of uniform-quadratic form, which is a proper norm of L_2-space and is helpful in the design of the difference scheme. Defining some elementary finite-difference and average operators, the discrete analogues of Eqs. (3)–(4) can be defined on the "C-grid" (for details, see [2]). It is not difficult to prove that the discrete system still preserves the major integral properties (5)–(6) of the differential system [4].

In order to save computing time, a splitting method is adopted in the model, with which the governing equations are divided into three stages [2]. The adjustment stage includes the elevation gradient and Coriolis terms which describe gravity–inertia oscillations. The development stage consists of the advection terms; and the forcing-dissipation stage consists of the wind stress and bottom friction terms. The three stages are integrated consecutively and the results of a previous stage are taken as the initial values for the next stage. In each cycle, the adjustment stage is integrated M times with a time step Δt, which satisfies the CFL condition, and is followed by the development and forcing-dissipation stages, which are integrated one time with the same time step $\Delta T = M\Delta t$. In practice, the value of M is often chosen as a factor of 5–10 (see Section 4).

3. FORMULATION OF THE OBCS

For convenience of the treatment of boundary conditions, open boundaries are usually placed along coordinate axes. Since all boundaries are treated in a similar fashion, it will be sufficient to look at the right-side boundary in the following.

3.1. *OBCs for the Adjustment Stage*

The finite-difference equations are integrated from time level t_n to level $t_{n+1} = t_n + \Delta t$. Thus we may linearize the split governing equations for the adjustment stage in the time interval $[t_n, t_{n+1}]$ as

$$\frac{\partial U}{\partial t} - fV = -c\frac{\partial \phi}{\partial x} \tag{7}$$

$$\frac{\partial V}{\partial t} + fU = -c\frac{\partial \phi}{\partial y} \tag{8}$$

$$\frac{\partial \phi}{\partial t} + \frac{\partial cU}{\partial x} + \frac{\partial cV}{\partial y} = 0, \tag{9}$$

where U, V denote the components of $\mathbf{V}$, and c is the value of Φ at time level t_n; i.e., c is time-independent in $[t_n, t_{n+1}]$.

The characteristic equations along the outward and inward characteristics for the system (7)–(9) are obtained, viz.,

$$\frac{\partial}{\partial t}(U+\phi) + \frac{dx}{dt}\frac{\partial}{\partial x}(U+\phi) = fV - U\frac{\partial c}{\partial x} - \frac{\partial cV}{\partial y} \quad \text{along} \begin{cases} dx/dt = c \\ dy/dt = 0 \end{cases} \tag{10}$$

$$\frac{\partial}{\partial t}(U-\phi) + \frac{dx}{dt}\frac{\partial}{\partial x}(U-\phi) = fV + U\frac{\partial c}{\partial x} + \frac{\partial cV}{\partial y} \quad \text{along} \begin{cases} dx/dt = -c \\ dy/dt = 0. \end{cases} \tag{11}$$

In order to minimize reflections, similar to [5], the slope of the inward characteristic (defined by $dx/dt = -c$ at the right-side boundary) is forced to zero at the boundary. Thus integrating (11) along $dx/dt = 0$ and using (10) to solve for $(\partial U/\partial t)$ and $(\partial\phi/\partial t)$, it follows that

$$\frac{\partial U}{\partial t} = -\frac{1}{2}c\frac{\partial}{\partial x}(U+\phi) + fV \tag{12}$$

$$\frac{\partial \phi}{\partial t} = -\frac{1}{2}c\frac{\partial}{\partial x}(U+\phi) - U\frac{\partial c}{\partial x} - \frac{\partial cV}{\partial y}, \tag{13}$$

to be obeyed at the right-side boundary. The time rate of change of the tangential velocity $(\partial V/\partial t)$ is given by Eq. (8). Using one-sided differences to replace the terms containing derivatives with respect to x, the discrete analogues of (12), (13) and (8) are derived, with which the boundary values of U, V, and ϕ at the time level t_{n+1} are obtained from data within and on the boundary.

3.2. *OBCs for the Development Stage*

As in the previous subsection, the split governing equations for the development stage are linearized as

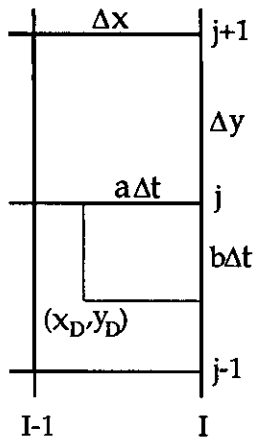

FIG. 1. Grids near the right-side boundary.

$$\frac{\partial \tilde{V}}{\partial t} + a\frac{\partial \tilde{V}}{\partial x} + b\frac{\partial \tilde{V}}{\partial y} + \mu\tilde{V} = 0, \quad t \in [t_n, t_{n+1}], \tag{14}$$

where $\tilde{V}$ represents U or V; $a = u^n$, $b = v^n$, and $\mu = \frac{1}{2}(\partial u/\partial x + \partial v/\partial y)^n$.

For a fixed point on the boundary, a, b, and μ are constants and will be maintained in the process of the solution, which is

$$\tilde{V}(x, y, t) = e^{-\mu t} A(x - at, y - bt), \tag{15}$$

where A is an arbitrary differentiable function, and a, b, and μ take values at point (x, y). At a point (x_I, y_j) on the right-side boundary, for instance, we have the formula to invert iteratively,

$$\begin{aligned} \tilde{V}_{I,j}^{n+1} &= \tilde{V}(x_I, y_j, t_n + \Delta t) \\ &= e^{-\mu(t_n+\Delta t)} A(x_1 - a\Delta t - at_n, y_j - b\Delta t - bt_n) \\ &= e^{-\mu\Delta t} e^{-\mu t_n} A(x_D - at_n, y_D - bt_n) \\ &= e^{-\mu\Delta t}\tilde{V}(x_D, y_D, t_n), \end{aligned} \tag{16}$$

where $x_D = x_I - a\Delta t$, $y_D = y_j - b\Delta t$.

When we know the values of $\tilde{V}^n$ at all points, we can obtain the values of $\tilde{V}^{n+1}$ at boundary points with the aid of the semi-Lagrange scheme (16). If $a > 0$ (at outflow points), (x_D, y_D) is located within the computational domain (Fig. 1), the value of $\tilde{V}^n$ at (x_D, y_D) can be calculated by using interpolation techniques; otherwise, if $a < 0$ (at inflow points), similar to [6], we let $a = 0$ so that the boundary will not be influenced by the external solution.

For the forcing-dissipation stage no boundary conditions are necessary.

4. NUMERICAL EXAMPLES

In order to test the stability and accuracy of the computational scheme and the efficiency of the proposed OBCs, two numerical experiments are described below.

4.1. *Restoration under Gravity in an Infinitely Long Channel*

This experiment is designed to test the ability of the proposed OBCs to allow propagating waves and advection to pass through open boundaries. To be considered is an ocean confined in an infinitely long channel of constant width. OBCs are applied at two artificial boundaries marked A-A and B-B in Fig. 2a. The depth of the channel is a function of the cross channel coordinates only (see Fig. 2b), so as to generate dispersive as well as nondispersive long waves.

The waves are stimulated by an initial bell-shaped swell in the surface elevation in the middle of the channel (the top of the swell is one meter higher than the mean sea level). In this simulation, no forcing is applied and the restoration was accomplished by dispersive shelf waves and nondispersive Kelvin waves propagating outwards from the initial swell. The IAP shelf sea model and the OBCs presented in the last section were utilized to perform the simulation. The model domain is a rectangle of 500 × 1000 km (Fig. 2), in which the grid spacing is taken uniformly as 10 km. In this example the forcing-dissipation stage is absent. The time steps in the adjustment and development stages are chosen as 180 s and 900 s, respec-

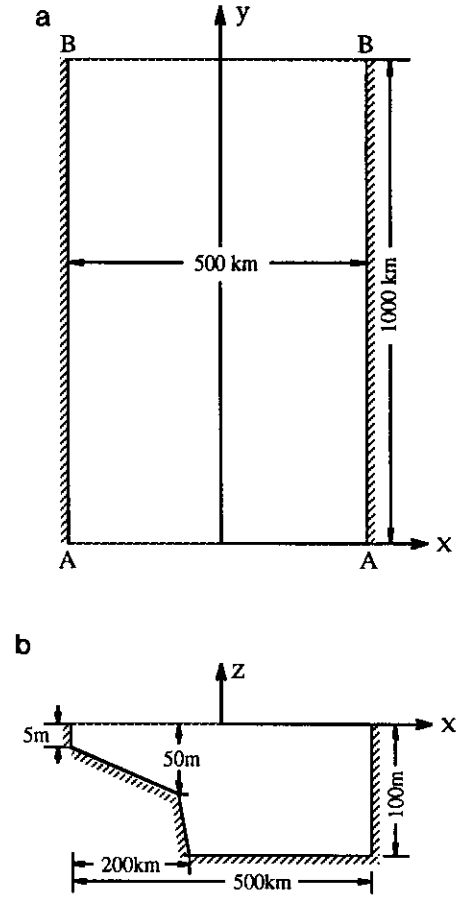

FIG. 2. Sketch of the channel. (a) Top view; (b) Cross section.

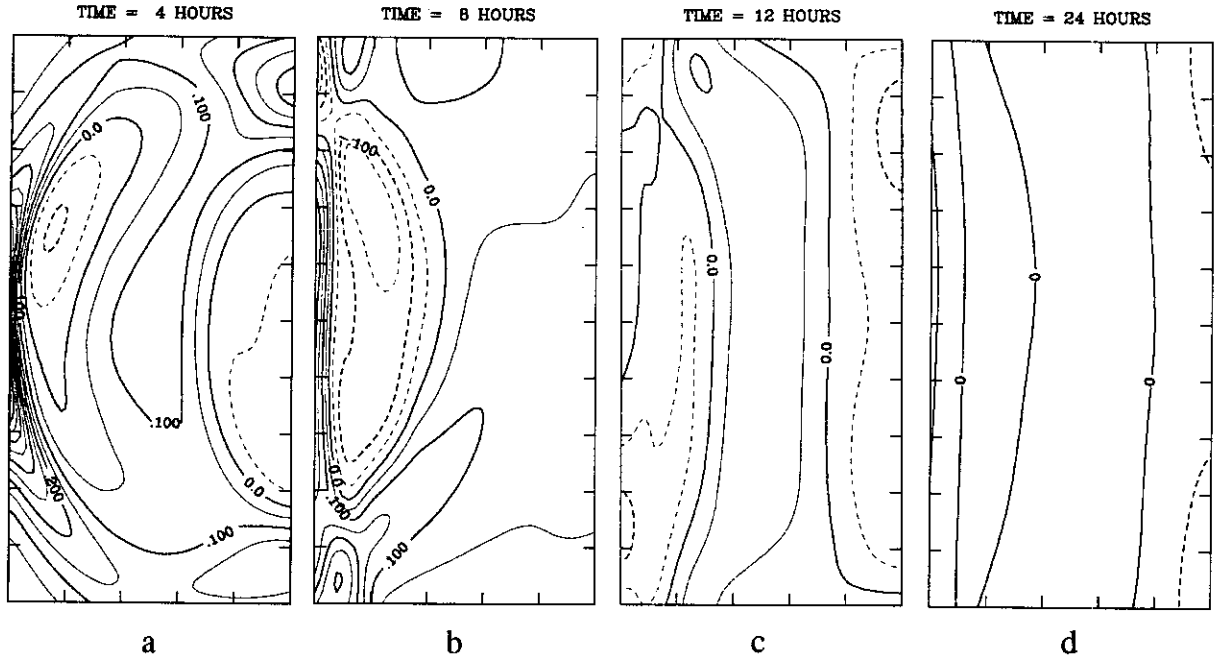

FIG. 3. Snapshots of sea surface elevation using the extended grid. Only the subdomain corresponding to the regular grid is shown. Dashed curves indicate depressions. Contour interval is 0.05 m.

tively. Other parameters used in the simulation are $\rho = 1025$ kgm^{-3}, $f = 7.29 \times 10^{-5}$ s^{-1}, $g = 9.81$ ms^{-2}.

Since no analytical solution is possible for this case, a numerical solution was derived by extending the model domain so far to the north and to the south that the solution within the regular grid cannot be affected by any lateral boundary reflections within the 24-h integration period. The solution in this extended grid is shown in Fig. 3, which illustrates the sequence of events. Figure 3a shows the fronts, originated by Kelvin waves, moving toward the artificial boundaries. Shelf waves also have been generated and trapped to the shelf after 4 h. After 24 h, all the waves have left the domain and most of disturbances have vanished. For comparison, the solution in the regular grid, with OBCs applied at the artificial boundaries, is displayed in Fig. 4. It is shown that all waves generated in the channel are reasonably accurately simulated to propagate out of the region.

4.2. Steady Response of an Open Sea to a Stationary Cyclone

Consider a constant-depth sea with a straight coast on the west and let (x, y) be rectangular coordinates such that the y-axis is along the coast; the linearized governing equations and boundary conditions are

$$\frac{\partial \boldsymbol{\nu}}{\partial t} + f(\mathbf{k} \times \boldsymbol{\nu}) = -g\nabla\zeta - \gamma\boldsymbol{\nu} + \boldsymbol{\tau}/\rho H \tag{17}$$

$$\frac{\partial \zeta}{\partial t} + H\nabla \cdot \boldsymbol{\nu} = 0 \tag{18}$$

$$x = 0, u = 0; \quad (x, |y|) \to \infty, (u, \nu, \zeta) \to 0. \tag{19}$$

Suppose that there exists a stationary axisymmetric cyclone whose center is at the origin of the coordinates, the distribution of the wind stress may be expressed as [7]

$$\tau_x = -\tau_{\max}(r/R)^2 e^{2(1-r/R)} \sin\theta, \quad \tau_y = \tau_{\max}(r/R)^2 e^{2(1-r/R)} \cos\theta,$$

where $r = \sqrt{x^2 + y^2}$, $\theta = \text{arc tg}(y/x)$. We have obtained, from (17)–(19), the exact steady-state solutions of the current velocity and sea-surface elevation along the coast, viz.,

$$\nu(0, y) = \frac{1}{\pi}\int_0^\infty \frac{rA(r)}{y} \ln\left|\frac{r-y}{r+y}\right| dr$$

$$\zeta(0, y) = -\frac{\gamma}{g}\int_0^y \nu(0, y)\, dy,$$

where

$$A(r) = \frac{\tau_{\max}}{\rho\gamma HR}[3(r/R) - 2(r/\mathrm{R})^2] e^{2(1-r/R)}.$$

The computational domain is a rectangle of 500 × 1000 km

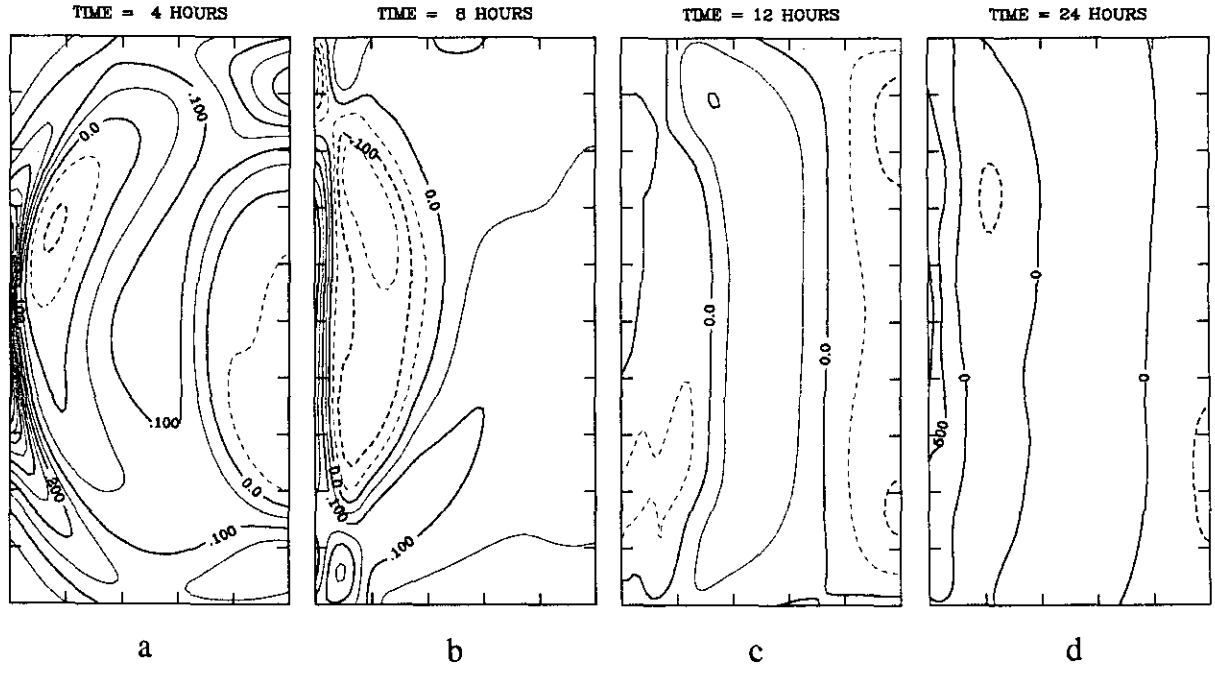

FIG. 4. Same as Fig. 3 except for using the regular grid.

(Fig. 5), where one boundary is closed and treated with a free-slip boundary condition and the other three margins are treated with OBCs. In this case, only the adjustment and the forcing-dissipation stages are included, and the time steps are taken as 180 s and 900 s, respectively. Other parameters are the same as that in the last example, except for $\tau_{max} = 2.4 N m^{-2}$, $R = 50$ km, $\gamma = 5 \times 10^{-5}\ s^{-1}$, $H = 50$ m.

Although the flow is time-independent, we still use the time-dependent equations to perform the calculation, take the solution which has reached a steady state as the numerical steady-state solution, and then compare it with the analytical one. After the run was made for 48 h the solution had reached its steady state, indicating that the difference scheme with the OBCs has good computational stability. The comparison of numerical and analytical solutions is illustrated in Fig. 6. Figures 6a and 6b show the distributions of the sea-surface eleva-

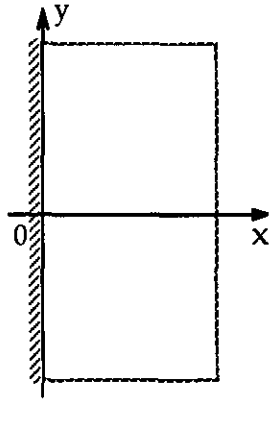

FIG. 5. Computational domain with the coordinates.

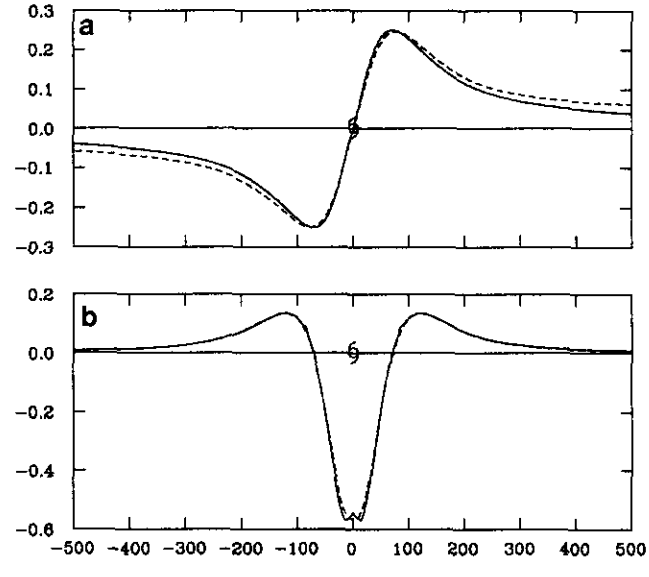

FIG. 6. Comparison of numerical (dashed line) and analytical (solid line) solutions. The abscissa denotes the distance along the coast (km): (a) sea-surface elevation (m); (b) current velocity (m/s).

tion and the current velocity along the coast, respectively. It can be seen that the numerical solutions coincide very well with the analytical ones.

5. CONCLUDING REMARKS

We have introduced in this paper OBCs that are suitable for the split scheme adopted by the IAP numerical shelf sea model. Good performance has been obtained for the cases studied. It should be noted that the idea proposed here may be extended to other split schemes and that extending the OBCs to baroclinic models remains for further work.

REFERENCES

1. Q.-C. Zeng, Z.-Z. Ji, and R.-F. Li, *J. Hydrodyn.* **2**, 1(1989).
2. Q.-C. Zeng, Z.-Z. Ji, and R.-F. Li, in *Frontiers in Atmospheric Sciences,* edited by Institute of Atmospheric Physics, Chinese Academy of Sciences (Allerton, New York, 1993), p. 208.
3. Q.-C. Zeng *et al.*, *Chinese J. Atmos. Sci.*, **13**, 127 (1989).
4. D.-J. Guo, Q.-C. Zeng, and Z.-Z. Ji, *Chinese J. Atmos. Sci.* **16**, 189 (1992).
5. K. W. Thompson, *J. Comput. Phys.* **68**, 1 (1987).
6. A. L. Camerlengo and J. J. O'Brien, *J. Comput. Phys.*, **35**, 12 (1980).
7. M. S. Longuet-Higgins, *Deep-Sea Res.* **12**, 923 (1965).